Title

A MEASURING SYSTEM FOR STUDYING THE TIME-RESOLUTION CAPABILITIES OF FAST PHOTOMULTIPLIERS

Authors

Lo, C.C.
Leskovar, B.

Publication Date

1973-11-01

Presented at IEEE Nuclear Science
Symposium, San Francisco, Ca.,
November 14-16, 1973

LBL-2423

A MEASURING SYSTEM FOR STUDYING THE TIME-RESOLUTION CAPABILITIES OF FAST PHOTOMULTIPLIERS

C. C. Lo and B. Leskovar

November 1973

Prepared for the U. S. Atomic Energy Commission
under Contract W-7405-ENG-48

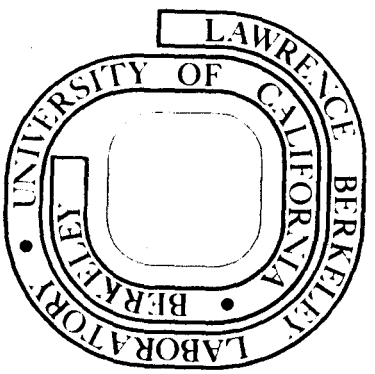

LBL-2423

DISCLAIMER

A MEASURING SYSTEM FOR STUDYING THE TIME-RESOLUTION CAPABILITIES OF FAST PHOTOMULTIPLIERS

C. C. Lo and B. Leskovar

Lawrence Berkeley Laboratory
University of California
Berkeley, California 94720

Abstract

A measuring system has been developed for studying and optimizing the time-resolution capabilities of fast photoelectric devices, such as standard and microchannel type photomultipliers. The system incorporates a subnanosecond light-pulse generator capable of operating at repetition frequencies up to 3 MHz with output light pulses having a full width at half-maximum of less than 200 psec, and a zero-crossing discriminator which has a time walk of ±40 psec over a 170 mV to 8 V input-pulse amplitude variation. Averaging the data from several successive measurements, the measuring system time resolution is 20 psec.

Introduction

Investigation of the time-resolution capabilities of fast photoelectric devices is becoming increasingly important in a multitude of research areas, such as subnanosecond fluorescence spectroscopy instrumentation, experimental research instrumentation, optical ranging experiments, and optical communication. The objective of our investigations is to determine and optimize the operating conditions giving the best time resolution with fast standard and microchannel type photomultipliers. These devices are important in subnanosecond nuclear lifetime studies and fluorescence spectroscopy instrumentation for biological research. Sensitivity and time response of single-photoelectron delay coincidence-time spectroscopy systems for lifetime measurements depend primarily on time capabilities of the photomultipliers and on the performance of a subnanosecond light source and signal processing system.[1]

Our measurements have shown that subnanosecond time-resolution capabilities of modern high-gain photomultipliers, such as single-electron time spread, are so good that the rise time and the full width at half maximum of the light pulse, as well as discriminator timing errors, have significant influence on measured results.[2-6] The study of these limiting factors has required the development of a special measuring system to study and optimize the time-resolution capabilities of fast photomultipliers.

Measuring System Block Diagram

A block diagram of the measuring system for studying the time-resolution of fast photoelectric devices is shown in Fig. 1. The system consists of a light pulse generator, a zero-crossing timing discriminator, leading edge discriminators, delay cables, time-to-pulse amplitude converter, and a multichannel analyzer. Since all components used in the system are available commercially, except the subnanosecond light pulse generator and the zero crossing timing discriminator, which play the most important roles in the whole system, this paper will treat these devices in considerable detail. An electroluminescent diode, Ferranti type XP-23, driven by an avalanche transistor pulse generator, was used as the light source. Generally, the photomultiplier time resolution studies were made with a small 1.6 mm light spot as functions of the position on the photocathode sensing area, and also with a large spot illuminating the full photocathode. For studies concerning different photocathode sensing areas, a positioning disc with 3.2 mm holes spaced 4 mm apart, along lines parallel to and perpendicular to the long axis of the first dynode, was attached to the photomultiplier window. To prevent the electromagnetic field of the light pulser from interfering with photomultiplier operation, a 12-inch long American Optical LG3 light guide was used to carry the light pulse to the photocathode. Whenever a particular area of the photocathode was chosen to be illuminated, the light guide was placed in the corresponding hole of the positioning disc. The successive scanning was done along the X and Y axes, with the longer side of the rectangular first dynode as the X axis. The illuminated area of the photocathode was no larger than 1.6 mm in diameter. For time resolution studies with full photocathode illumination, the positioning disc was removed. For measurements of photomultiplier C31024, an auxiliary anode bias supply, a variable attenuator, and wideband amplifiers, Hewlett Packard Type 8447F, were inserted at points a and b. The auxiliary anode bias supply was needed for obtaining linear anode pulse currents of approximately 75 mA peak from the C31024. The discriminator output was applied to a time-to-height converter via a discriminator-pulse shaper. The reference time pulse was obtained from the light pulser and was passed through a delay line and a discriminator. The discriminator was followed by the time-to-height converter whose output pulses were applied to a 400-channel pulse-height analyzer.

Subnanosecond Light Pulse Generation Considerations

A critical evaluation of the measuring system has shown that the full width at half maximum of the light pulse is a fundamental limitation of the measuring system time resolution. For an accurate measurement of time resolution, particularly single electron time spread, the width of the light pulse should be as small as possible in comparison with the value of the single electron time spread. Otherwise, the light pulse width will contribute directly to the amount of the electron time spread. This is particularly important in situations where operating conditions of a photomultiplier are optimized to obtain a minimum value of the electron time spread. Our measurements have shown that, for a standard contemporary type photomultiplier with properly optimized operating conditions, the electron time spread is typically 320 psec for small illuminated areas.[5,6] Our preliminary measurements have shown that a typical value for a microchannel-type photomultiplier is 150 psec, without optimization of its operating conditions. Therefore, the light pulse generator should be capable of supplying the subnanosecond light pulses with a frequency spectrum appropriately matched to the photocathode spectral response. The pulse repetition frequency should be as high as possible.

Electroluminescent Diode as Subnanosecond Light Source

In earlier published works,[7-10] application of solid-state light emitting sources were described, particularly gallium arsenide and gallium phosphide electroluminescent diodes. Using a mercury reed pulser, a full width at half-maximum of approximately 0.5 nsec was obtained at a pulse repetition frequency of 60 Hz. The Cerenkov radiation process has also been used for producing short light pulses.[11] However, the process is characterized by relatively low intensity and pulse repetition rate. Furthermore, the Cerenkov radiation process does not provide any convenient electrical trigger signal for associated electronic circuits.

In the present work, forward-biased and reverse-biased alloyed junction electroluminescent diodes were investigated as sources for subnanosecond light pulses. Generally, an electroluminescent diode emits light within the photocathode spectral response of most photomultipliers used for nuclear pulse counting. However, the relative degree of overlap occurring between the photocathode spectral response and the spectral distribution of the diode-emitted light varies widely, depending upon the particular photocathode, electroluminescent diode, and diode operating conditions. The dimensionless spectral matching factor, as defined in Ref. 12, enables one to calculate the degree of overlap, and to determine photocathode current for a given electroluminescent diode. The matching factor is expressed as the ratio of the area under a curve, defined by the product of the relative spectral curves of the electroluminescent diode and photocathode, to the area under the diode relative spectral curve. This relationship can be expressed mathematically as:

$$M = \frac{\int_0^\infty W(\lambda)R(\lambda)\,d\lambda}{\int_0^\infty W(\lambda)\,d\lambda} ,$$

where $W(\lambda)$ is the spectral characteristic of the diode normalized to unity, and $R(\lambda)$ represents the photocathode spectral response as a function of wavelength, normalized to unity at the peak.

To determine electroluminescent diode-photomultiplier spectra matching factors, the relative spectral characteristics of a forward-biased and reverse-biased gallium phosphide diode, Ferranti type XP-23, were measured and compared with the published spectral response of semitransparent bialkali and extended-red multialkali photocathodes. The diode spectral characteristics were measured with a Jarrell-Ash f6 Spectrograph, recorded on Kodak spectroscopic plates, type 103aF and type 1N, which were measured with a Jarrell-Ash 23-100 Microphotometer, and the spectral response plotted. Results of these measurements are given in Figs. 2 and 3. The matching factors for RCA photomultipliers 8850, C31024, and C31000E for the forward bias case were calculated, according to Equation (1), to be 0.023, 0.026, and 0.722, and for the reverse-biased diode 0.050, 0.052, and 0.813, respectively. It can be seen that reverse-biased electroluminescent diodes have a higher spectral matching factor with typical bialkali and multialkali photocathodes than forward-biased diodes. A forward-biased Monsanto type diode MV10A gave matching factors of 0.0013, for types 8850 and C31024, and 0.808 for type C31000E.

Further measurements on a number of XP-23 diodes showed that there is a significant difference in the emitted light pulse, depending upon whether the diodes are excited in the forward or reversed direction, as can be seen from Figs. 4 and 5. Using a fast photomultiplier RCA C31024 as a detector, the impulse excitation of the diode by a 3A, 250 psec current pulse in the forward direction resulted in a train of amplitude decaying light pulses which lasted for approximately 300 nsec, due to the long storage time. The impulse excitation in the reverse direction by the same electrical

pulse as in the previous case gave a clean light pulse, as can be seen from Fig. 5. Using an RCA 31000E as a detector, the output pulses showed the similar pattern for forward and reverse impulse excitation. Also, impulse excitation with 120 mA, 5 nsec current pulses gave photomultiplier output pulses of similar structure as in the previous case. Consequently, the reverse impulse excitation of the electroluminescent diode was used in the subnanosecond light pulse generator, both because of the higher matching factor and the clean waveshape of the light pulse. The Monsanto gallium arsenide phosphide MV10A diode did not show different waveshapes of the light pulse under forward or reverse impulse excitation. However, it was not used in our measurements because of significantly lower values of the spectral matching factor for a typical bialkali photocathode.

Photoelectron Yield Measurements

The photoelectron yield per excitation impulse in the reverse direction was measured for the XP-23 diode, using photomultiplier types C31024 and 8850 with bialkali photocathode, and a C31000E having an extended red multialkali photocathode as detectors. With the system diagrammed in Fig. 6, the photoelectron yield was measured as a function of electroluminescent diode pulse current, with current pulse width as the parameter.

The electrical pulse was generated by a Tektronix 110 pulse generator. The current amplitude of the electrical pulse was adjusted by varying an external dc power supply, and the width of the electrical pulse was determined by the length of the charging line used. To obtain the 250 psec FWHM electrical pulse, the General Radio connector at the rear panel of the Tektronix 110 pulse generator was disconnected inside the generator from the charging circuit, thus reducing the length of the charging line to a minimum. The electroluminescent diode current was monitored by using a Tektronix P6034 probe connected across a current shunt in series with the diode. The current shunt was made up of six 10 ohm 1/4 watt carbon composition resistors arranged in a concentric manner with the XP-23 diode assembly, with a "Conhex" bulkhead receptacle, type 15, mounted at the center.

The photocathode of the photomultiplier was placed one inch away from the diode to capture nearly all of the photons from the diode. The peak of the single photoelectron pulse height spectrum on the multichannel analyzer was first located and used as the reference channel. Once this was done, the photomultiplier operating conditions remained the same throughout the experiment; this was essential to eliminate the uncertainty of the photomultiplier gain which, if changed, undoubtedly would affect the accuracy of the measurement. The maximum anode output current of the photomultipliers throughout the whole measurement was kept below 25% of the peak linear anode current to ensure good linearity. Since the amount of photoelectron yield per pulse extended over more than four decades, it was necessary to attenuate the light intensity accurately. This was done with calibrated optical neutral density filters. Since noise pulses in these photomultipliers were single-electron dominated, the noise pulses were used to locate the single photoelectron peak. This was done with the electroluminescent diode turned off and the linear gate opened to allow noise pulses to go through. After the peak was located, the gate was enabled to reject almost all other pulses except those generated by the diode. The driving current of the diode was adjusted so that the output pulses from the photomultiplier were single-electron dominated. This was the pulse current producing one photoelectron. The counting rate and the pulse height were noted at this time and used as a reference for further measurements. A neutral density filter with 10% transmittance was then inserted between the diode and the photomultiplier, and the driving pulse current of the electroluminescent diode was adjusted to bring back the same counting rate and pulse height as in the previous case. This was the pulse current producing 10 photoelectrons. A 1% transmittance neutral density was then placed between the photocathode and the diode, and the diode driving pulse current was again adjusted to obtain the same counting rate and pulse height. This was the pulse current producing 100 photoelectrons. Likewise, a 0.1% transmittance neutral density filter was used to calibrate a diode pulse current corresponding to 1000 photoelectrons. The same technique was used for all three photomultipliers. Results of the measurement are shown in Figs. 7, 8 and 9. The yield of photoelectrons per pulse is nearly proportional to the breakdown current over two to three decades of current, for electrical pulse widths of 5 and 10 nsec. There is a nonlinear dependence of photoelectron yield upon the breakdown current for electrical pulse widths of 0.25 nsec, 0.5 nsec, and 1 nsec.

The peak inverse voltage across the diode is of interest. With the photomultiplier type C31024 and an electrical pulse width of 5 nsec, a voltage of 37 V at 3 A resulted in a photoelectron yield value of 10^3 per pulse. When a photomultiplier type 8850 was used with the same pulse width and photoelectron yield, the peak diode voltage and current were 34 V and 2.4 A, respectively. For an electrical pulse width of 250 psec, a peak voltage value of 66 V at 3.6 A of pulse current produced a photoelectron yield of 40 for the C31024. When an 8850 was used, a peak voltage value of 50.5 V at 2.7 A of pulse current gave the same result. Using a C31000E, the peak voltage value was 30.8 V at 1.9 A of pulse current for the photoelectron yield of 10^4, using a pulse 5 nsec wide. The peak reverse voltage value was 55 V at 3 A of pulse current for the photoelectron yield of 400 and an electrical pulse width of 250 psec.

Although literature dealing with explanations of physical phenomena of light emission from forward-biased p-n junctions (recombination radiation) is extensive,[13,14] there is no satisfactory explanation of fast pulse light emission from reverse-biased gallium phosphide junctions (breakdown radiation).

In general, reverse-bias electroluminescence in GaP diodes can be associated with the internal-field emission (Zener) process, and avalanche breakdown. In the internal-field emission process, the slope of the conduction and valence bands in the depletion layer becomes so steep that the horizontal distance between the isoenergetic levels lying in the valence and conduction bands becomes smaller than 100 A. Under these conditions, electrons can pass through the forbidden gap into the conduction band by the quantum-mechanical tunneling mechanism.

The avalanche breakdown process occurs in practical diodes when the junction electric field becomes approximately 10^6V/cm. In this case, electrons and holes contributing to the total junction saturation current attain sufficient kinetic energy in the depletion layer to cause impact ionization of the valence electrons. These electrons are promoted to the conduction band through electron-electron scattering. The secondary electrons produced in this way are accelerated to produce more carriers by impact ionization. Breakdown occurs because of the rapid increase in the carrier density due to the avalanche multiplication process.

Avalanche breakdown can be distinguished from tunneling breakdown by an analysis of the reverse bias I-V characteristics and their temperature dependence. The temperature coefficient of the breakdown voltage, dV_B/dT, is negative for the tunneling mechanism because the energy band decreases with rising temperature. For an avalanche breakdown the temperature coefficient is positive, because the free path of hot carriers decreases with rising temperature, due to the excitation of optical phonons. Our measurements of the temperature coefficient of the diode XP-23, made at temperatures of 77°K and 300°K, have shown a decrease of the breakdown voltage with decreasing temperature, indicating a genuine avalanche breakdown. The diode breakdown voltage was approximately 10 V at 300°K.

GaP diode electroluminescence originates in small avalanche breakdown regions in the junction plane (so called microplasmas) which occur at local inhomogeneities in the junction field. The field inhomogeneities are caused by crystal imperfections. Microplasmas have been associated with groups of dislocations or dislocations in regions of doping inhomogeneity. The quantum efficiency of the reverse bias electroluminescence is generally low, because the electron-hole pairs generated by impact ionization are separated by the external field, and the recombination probability of the energetic carriers is low. However, as described in a previous section, reverse bias electroluminescence gives a clean light pulse with extremely short rise and decay time. The short rise and decay time is not surprising, since the time constants for the buildup of an avalanche process are extremely small, depending primarily upon carrier scattering time. Moreover, when the current pulse is turned off, the built-in junction field sweeps the carrier into the n- and p-region. There they are the majority carrier and cannot give rise to radiative recombination. Consequently, it can be said conclusively that the FWHM of of the emitted light pulse is closely equal to the FWHM of the diode current pulse.

Concerning the reverse-bias electroluminescence spectra, it would appear from the results presented in Ref. 15 that the bremsstrahlung mechanism is a possible explanation for the radiation spectra that have been observed. In this mechanism the high-energy carriers lose their energy at breakdown by retardation in the Coulomb field of ionized impurities, causing the emission of light.

Our measurements have shown that the low-intensity light was emitted from the electroluminescent diode in the prebreakdown region of the dc diode current-voltage characteristics. The measured threshold of the dc reverse voltage applied to an electroluminescent diode XP-23, for single-photoelectron emission, had an average value of 6.1 V for 9 diodes. The average value of the diode current was 0.55 μA. The average value of the dc forward voltage threshold for single-photoelectron emission was 1.33 V. The average value of the diode current was 0.88 mA. In these measurements the photomultiplier C31000E was used as a detector.

Subnanosecond Light Pulse Generator

The subnanosecond light pulse generator developed with electroluminescent diode XP-23 is shown in Fig. 10. The circuit designed to provide the operating subnanosecond current pulses for the diode consists of an avalanche transistor pulse generator and a step recovery diode pulse-shaping unit to steepen the front edge of the electrical pulse. A separate standard type pulse generator, capable of supplying pulses with nanosecond rise-times and amplitudes between 1V to 5V, is required to operate the subnanosecond light pulse generator. The polarity of the input pulse is determined by the connection of the input pulse transformer. With an input trigger pulse, both avalanche transistors break down at the same time, discharging the energy stored in the emitter circuits of the avalanche transistors. The 10 to 1 resistor divider at the collector of the transistor Q_2 provides a trigger pulse for triggering external circuits. Through the 470 pf decoupling capacitor, American Technical Ceramics 100 B 471 M MS 200, the output pulse from the avalanche transistor stage is fed to the step recovery diode, HPA 5082-0320, which is biased in the forward direction. As the

negative charge from the pulse equalizes the positive charge stored in the diode, the diode snaps to the off state in approximately 100 psec. To further reduce the tail of the pulse, a 16 mm-long, 50Ω clipping stub is used. The two hot-carrier diodes connected in parallel block the dc path for the step recovery diode bias. Current waveforms, as monitored across the current shunt, showed ringing in the 2 GHz range. To investigate whether this ringing was producing photons, an RCA C31000E photomultiplier with extended red multialkali photocathode was used to monitor the photon emission from the XP-23 diode.

Normally, the electroluminescent diode was driven by a current pulse of -1.33 A having a width at FWHM of 200 psec, while the voltage across the diode was -20 V. The positive-ringing half cycle had an amplitude of +0.662 A, the width being 250 psec at FWHM, and the negative half cycle of the ringing had an amplitude of -0.3 A, having approximately the same width. To determine that the positive-ringing half cycle was not producing any photon, the Tektronix 110 pulse generator was used to find the current threshold of the diode when being pulsed in the forward direction. The current threshold barely starting to produce single photon emission, as seen by the C31000E, was +0.722 A with a 250 psec pulse. The negative half cycle ringing current of -0.3 A was well below the current threshold for producing single photons in the reverse direction of the impulse excitation. Furthermore, monitoring the output of the C31000E photomultiplier with an oscilloscope showed no objectionable pulses, such as those produced by operating the XP-23 diode in the forward direction of the impulse excitation.

To find the current threshold of the XP-23 diode for producing single photoelectrons in the reverse direction of the impulse excitation with a 200 psec pulse, the dc power supply of the subnanosecond pulse generator was lowered until no photon emission was detected. The negative current threshold was found to be -1.15 A, using a photomultiplier C31000E as a detector. The voltage across the diode at this point was -17.5 V. Furthermore, to make sure that the output pulses from the photomultiplier were of single-photoelectron origin, a pulse height spectrum was measured.

The subnanosecond light pulse generator was capable of operating at a repetition frequency of 3 MHz, with an output light pulse having approximately a full width at half maximum of less than 200 psec. The high repetition frequency is particularly desirable, since it shortens measuring time necessary for obtaining the required statistics for the study of time resolution capabilities of fast photomultipliers.

Zero-Crossing Discriminator

The time walk and resolution characteristics of a zero-crossing discriminator are perhaps the most important factors in determining the timing error of the measuring system. A number of circuits have been devised for deriving timing signals from scintillation detectors with a reduced amplitude-dependent timing error.[10] Of three methods for deriving time information from the photomultiplier output pulse, the leading edge timing with a fixed threshold discriminator, the fast cross-over timing, and the constant-fraction-of-pulse-height timing, our measurements and considerations show that the fast cross-over timing with the clipping stub technique[16] is at present the most practical method for single photoelectron timing. A modified-pedestal type discriminator was developed, in which the photomultiplier anode signal is clipped and a pedestal added, allowing adjustment of the discriminator to the zero-crossing point.

Generally, a bipolar pulse can be generated either by a clipping stub or by the attenuation-subtraction technique. The abrupt baseline crossover point of a bipolar pulse is relatively independent of the pulse amplitude, thus making it a good place to obtain the amplitude-independent timing information. Despite the amplitude-independent crossover point of a bipolar pulse, a leading edge detector being triggered at this point still introduces walk in the nanosecond range when the amplitude dynamic range is wide. To overcome this, a pedestal is added to shift the bias up to the detector threshold at the right time. By doing this, the detector triggers as soon as the zero-crossing point of the bipolar pulse is reached, producing an amplitude-independent timing pulse. In this discriminator, tunnel diodes with backward diode nonlinear loads were used exclusively as threshold devices and pulse shapers.

Circuit Description

A schematic diagram of the zero-crossing discriminator is given in Fig. 11. Pertinent waveforms at the specified points in the diagram and the discriminator sequence of operation are given in Fig. 12. Referring to both figures, the unipolar input anode pulse at point A has been changed to a bipolar pulse at point B by a clipping stub. The input signal connector and the clipping stub connector on the discriminator are connected directly to the circuitry without any length of coaxial cable in between. This is especially important for those short signal pulses which require a short clipping stub and minimum transit time termination. In fact, special efforts were made to minimize all interconnecting leads throughout the entire discriminator, which was built on a

carefully laid out double-sided fiberglass board. If there is ringing on the trailing edge of the input pulse, the zero-crossing point should be placed away from the ringing portion, or the signal should be improved before making measurements; otherwise the timing information will be impaired.

The termination and amplitude-limiting network consist of resistors R1, R2, R3, and diodes CR1 and CR2. The diodes make up the nonlinear part of the voltage divider, which attenuates high amplitude input pulses to prevent damage and to minimize time walk due to overloading of the zero-crossing and threshold detectors, CR4 and CR5. However, when the input pulse amplitude approaches 10 V, overloading time-walk becomes significant. Diodes CR1 and CR2, the nonlinear elements in the voltage divider, contribute partially to this undesirable shift in time. Resistors R4 and R5 constitute a 20 db attenuator, providing a monitor signal of the bipolar pulses.

The positive portion of the bipolar pulse serves as the trigger pulse for the tunnel diode CR4 threshold detector. Diode CR4 has a peak current of 4.7 mA. The abrupt cross-over slope provides better triggering for the leading edge threshold discriminator, resulting in a pedestal with less time shift due to the wide dynamic range of input signal pulse amplitude. Operating the leading edge threshold detector in this fashion, the pedestal time shift was found to be approximately 500 picoseconds better than the same detector triggering at the leading edge of the input signal pulse over a dynamic range of 30:1. Variable resistor R9 is the lower threshold adjustment of diode CR4, the control range being approximately from 30 mV to 3 V. Inductor L1 and a backward diode CR3 serve as the nonlinear load for tunnel diode CR4. Operating a tunnel diode in this mode improves performance in sensitivity and reduces standby power dissipation.[18] The output of this stage in turn triggers the tunnel diode CR8 which is the pedestal generator. Diode CR8 has a peak current of 10 mA. A shorting stub is the load for this stage, which generates a 15 nanosecond long pedestal (point C). While this is taking place, the bipolar pulse is being delayed for approximately 2.6 nanosecond by the delay cable (point D) before appearing across tunnel diode CR5, the zero-crossing detector. Diode CR5 has a peak current of 10 mA. Variable resistors R10 and R15 are for bias adjustment for the tunnel diode CR5 and the pedestal generator diode CR8, respectively. The bias pedestal is applied to the zero crossing detector diode CR5 through inductor L3 and resistor R14. Before the pedestal bias pulse reaches tunnel diode CR5, the bipolar pulse arrives and its negative-going portion ensures that the zero-crossing detector will not trigger until the zero crossover point is reached, at t_3. The zero-crossing detector is a one-shot multivibrator, using an inductor L2 and a backward diode CR7 as a nonlinear load. Resistors R12 and R13, R22 and R23 are voltage dividers providing monitoring signals for the zero-crossing detector and pedestal generator, respectively.

The buffer stage which follows uses tunnel diode CR10 and the primary winding of the coupling transformer and the backward diode CR11 as its nonlinear load. Diode CR10 has a peak current of 10 mA. Variable resistor R17 provides bias adjustment for CR10. Transistor, Q1, serves as the output amplifier. The output pulse at point F is a .5 V negative pulse with 7.5 nsec at FWHM and 1.5 nsec risetime. The total propagation time through the discriminator is approximately 10 nsec.

Time Charactersitics Measurements of Zero-Crossing Discriminator

Time walk and resolution characteristics of the zero-crossing discriminator, as a function of the input pulse amplitude, were measured with input pulse risetime and width as parameters.

A block diagram of the system for measuring discriminator time-walk characteristics is shown in Fig. 13. The source of input pulses was a HP215A pulse generator. Input signal pulses of 0.8 nsec rise time were applied to the discriminator through a wideband variable attenuator, in order to provide input signal pulses of variable amplitude. Where input signal pulses of a slower rise time were needed, a three-section RC integrator was used between the Tektronix P6034 probe and the variable attenuator. The reference timing signal was taken from a Tektronix probe to eliminate any time jitter from the signal generator.

The time walk of the attenuator was explored before the discriminator time walk was measured. For this purpose, an appropriate clipping stub was connected at the output of the HP215A pulse generator. The integrator was not in the circuit, as 0.8 nsec risetime pulses were used. The zero-crossover point of the bipolar pulse coming out from the attenuator was fed directly to one channel of the sampling oscilloscope, and was compared with the zero-crossover point of the reference pulse on the other channel. Using the 20 db position as the reference point, the time walk of the attenuator was found to be ±50 psec over an attenuation range of 40 db. When measuring the discriminator time walk, the integrator was used to obtain pulses with slower risetime and the clipping stub was removed from the output of the HP pulse generator. The time walk characteristics of the system were then found by comparing the 50% point of the leading edge of the reference pulse and the 50% point of the leading edge of the output pulse of the discriminator. Again the 20 db position was used as the reference point. The time walk characteristics of the discriminator were obtained by making corrections for time walk of the attenuator.

Time-walk characteristics of the discriminator, as a function of the input pulse amplitude with various input pulse rise times and widths as parameters, are shown in Figs. 14 and 15. The repetition frequency of the input pulses was 100 kHz. The input pulse rise time and width in Fig. 14 were 0.8 nsec, 1.5 nsec, 2 nsec, 4 nsec, and 1.3 nsec, 2.2 nsec, 3 nsec and 6 nsec, respectively. It can be seen from Fig. 14 that the time walk in the best possible case has a value from -40 psec to +40 psec for an input pulse amplitude variation from 170 mV to 8 V and an input pulse rise time and width of t_r = 0.8 nsec and t_w = 1.3 nsec, respectively. The time walk is from -60 psec to -40 psec for the same input pulse amplitude variations as in the previous case, where the input pulse rise time and width are t_r = 1.5 nsec and t_w = 2.2 nsec, respectively. The discriminator time-walk characteristics for input pulse width t_w = 10 nsec and input pulse rise time t_r = 0.8 nsec, 1.5 nsec, 2 nsec and 4 nsec are given in Fig. 15. It can be seen that the value of time walk varies from -40 psec to +40 psec for input pulse amplitude variations from 120 mV to 8 V and a pulse rise time of t_r = 1.5 nsec. Generally, the shapes of the time walk curves depend upon the input pulse rise time and width.

The block diagram of the system for measuring the time resolution of the zero-crossing discriminator is given in Fig. 16. The discriminator time resolution was measured as a function of the input pulse amplitude with the input pulse rise time and width as parameters. Similarly, as in the previous case, the Tektronix pick-off probe P6034 was used to obtain a reference pulse and to eliminate the jitter from the pulse generator. The reference pulse amplitude remained the same during the discriminator resolution measurements. To find the time resolution of the system without the zero-crossing discriminator, the discriminator was disconnected from the system. The measured time resolution of the system was 15 psec FWHM. With the discriminator in the system, and using the wideband attenuator to vary the input pulse amplitude, the time resolution of the complete system was measured. Results of measurements are given in Fig. 17. It can be seen that the total system time resolution is 20 psec FWHM, for an input pulse amplitude variation from 200 mV to 8 V and for a pulse rise time and width of 0.8 nsec and 1.3 nsec, respectively. The time resolution is below 80 psec FWHM for input pulse rise times of 2 nsec and 4 nsec for the same input pulse amplitude variation. Generally, the complete system time resolution is practically determined at low values of input pulse amplitude by the time resolution of the zero-crossing discriminator. Additional improvements of the time walk and resolution characteristics of the discriminator are possible by using a wideband precision type amplifier with a wide dynamic range.

Conclusions

Characteristics of a measuring system for studying the time resolution capabilities of fast electro-optical devices have been presented and discussed. A new subnanosecond light pulse generator and zero-crossing discriminator have been developed and employed in the measuring system to reduce pulse light width and amplitude-dependent time errors, when performing investigation and optimization of time-resolution capabilities of electro-optical devices. The timing errors associated with impulse pulse amplitude variations have been evaluated so that circuit parameters may be chosen to minimize these errors. The system can be modified and expanded to a number of practical situations where high time resolution in the subnanosecond region is needed. Furthermore, using the described system, determination of optimum operating conditions of fast photoelectric devices can be done easily and conveniently in a relatively short time.

By means of the described system, a single-photoelectron time spread of 320 psec FWHM has been measured for an RCA 8850 photomultiplier, using a 1.6 mm light spot on the photocathode, and optimizing the input electron optical operating conditions.

Acknowledgment

This work was performed as part of the program of the Physics-Chemical Biodynamics Instrumentation Research and Development Group of the Lawrence Berkeley Laboratory, Berkeley, and was supported by the U. S. Atomic Energy Commission, Contract No. W-7405-eng-48.

References

1. A. Weissberger, B. W. Rossiter, Physical Methods of Chemistry, Vol. 1 (Wiley-Interscience, New York, 1972), pp. 429-484.
2. C. C. Lo and B. Leskovar, Evaluation of the 8850 Photomultiplier with a Cesiated Gallium-Phosphide First Dynode, Lawrence Berkeley Laboratory, Engineering Note No. 1383, September 1971, University of California, Berkeley, California.
3. C. C. Lo and B. Leskovar, Evaluation of the C70133B Photomultiplier with a Cesiated Gallium-Phosphide First Dynode, Lawrence Berkeley Laboratory, Engineering Note No. 1387, October 1971, University of California, Berkeley, California.
4. C. C. Lo and B. Leskovar, Preliminary Results of Tests of the C31024 High Speed Photomultiplier with Cesiated Gallium-Phosphide Dynodes, Lawrence Berkeley Laboratory, Engineering Note No. 1384, October 1971, University of California, Berkeley, California.
5. B. Leskovar and C. C. Lo, Performance Studies of Photomultipliers Having Dynodes with GaP(Cs) Secondary Emitting Surface, IEEE Trans. Nucl. Sci., NS-19, No. 3, 60-72 (1972).
6. B. Leskovar and C. C. Lo, Single Electron Time Spread of Fast Photomultipliers, Lawrence Berkeley Laboratory Report LBL-968 (1973).
7. P. Leclerc and C. Zajde, Ultrafast Infrared Emitting Diodes, Review of Scientific Instruments, 36, 1056-7, July 1965.
8. P. Leclerc and M. Voos, Fast Infrared Light Pulse Generator, Journal of Scientific Instruments (Journal of Physics E), 1, 1968 Series 2, 478-9.
9. J. Johnson and D. Porat, Nanosecond Light Source, XP-20, Review of Scientific Instruments, 38, No. 12, 1796-8, December 1967.
10. Sherman K. Poultney, Single Photon Detection and Timing: Experiments and Technique, Advances in Electronics and Electron Physics, 31, Marton, ed., 39-117, 1972.
11. D. B. Scarl, Measurements of Photon Correlations in Partially Coherent Light, Physical Review, 175, No. 5, 1661-8, November 1968.
12. E. H. Eberhardt, Source-Detector Spectral Matching Factors, Applied Optics, 7, 2037-47, 1968.
13. P. R. Thornton, The Physics of Electroluminescent Devices, (E. & F. N. Spon Limited, London, 1967).
14. A. A. Berg and P. J. Dean, Light-Emitting Diodes, Proceedings of the IEEE, 60, No. 2, 156-224, February 1972.
15. J. Shewchun and L. Y. Wei, Mechanism for Reverse-Biased Breakdown Radiation in p-n Junctions, Solid State Electronics, 8, 485-493, (1965).
16. Donald L. Wieber and Harlan W. Lefevre, An Amplitude-Independent Nanosecond Timing Discriminator for Fast Photomultipliers, IEEE Trans. Nucl. Sci., NS-13, No. 1, 406-412, 1966.
17. S. L. Sarnot, On the Use of a Nonlinear Element in Tunnel Diode Circuits, Proceedings of the IEEE, 59, No. 1, 107-8, January 1971.

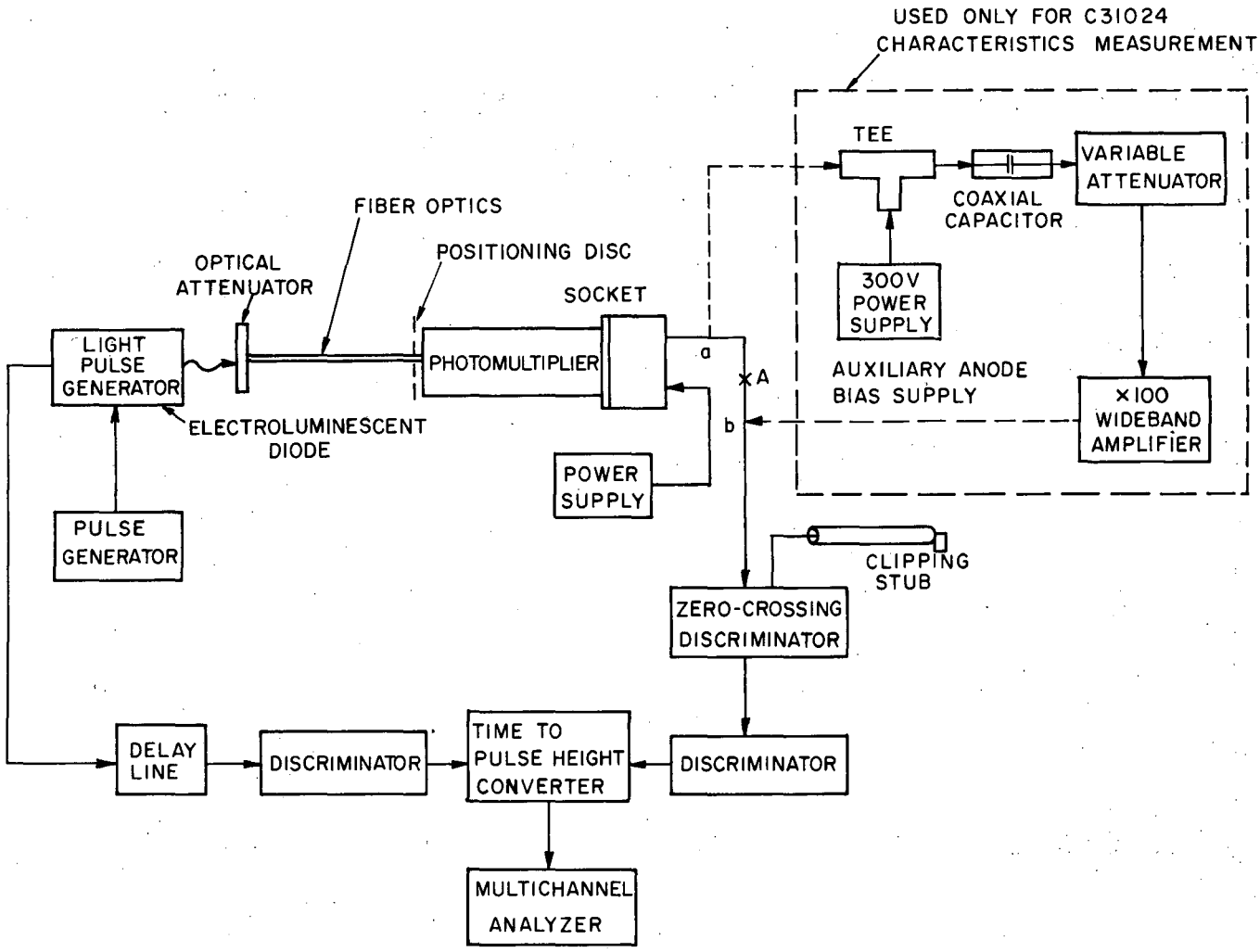

Fig. 1 Block diagram of the system for studying the time resolution capabilities of fast photomultipliers.

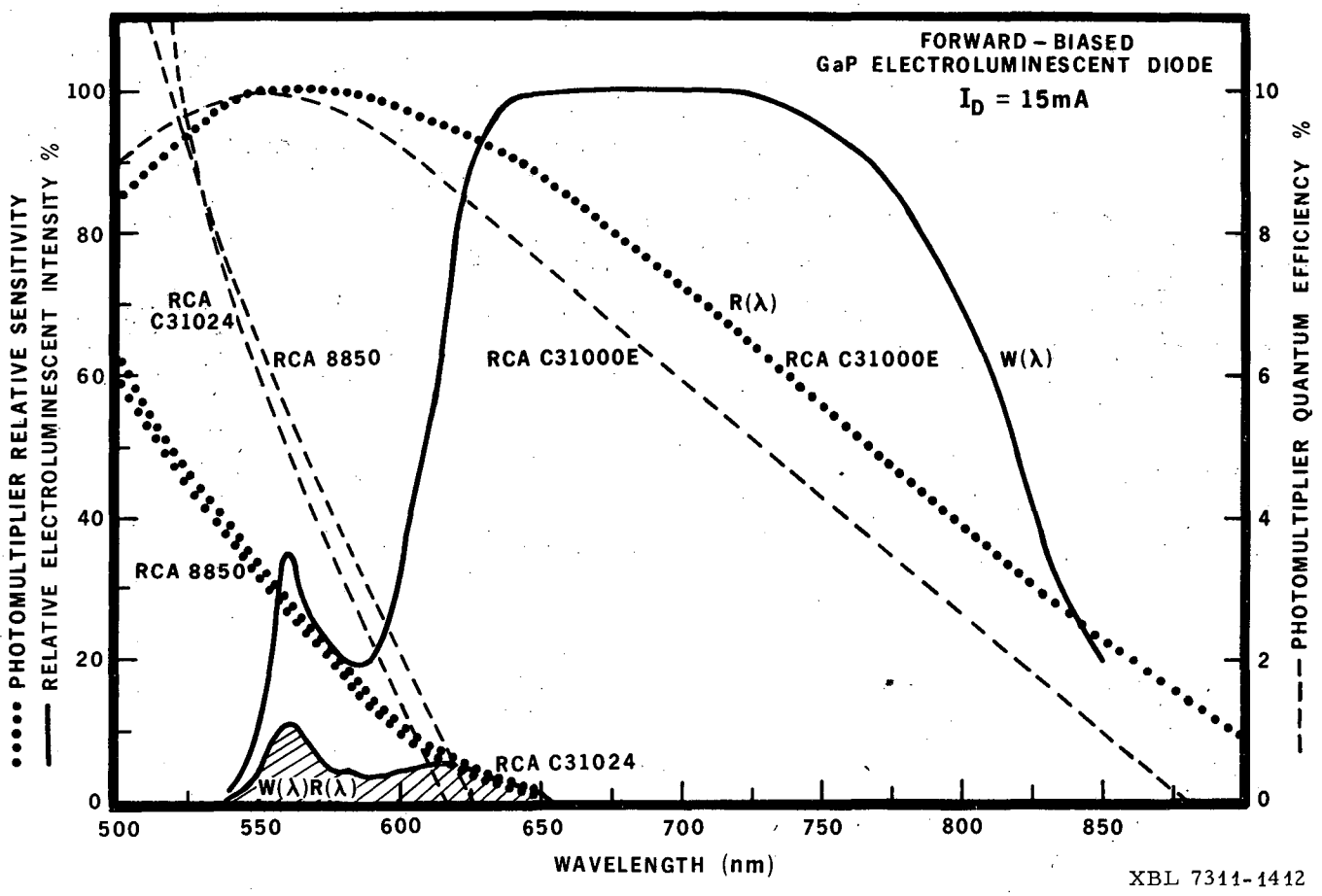

Fig. 2 Relative spectral characteristics of a forward-biased gallium phosphide electroluminescent diode, Ferranti XP-23.

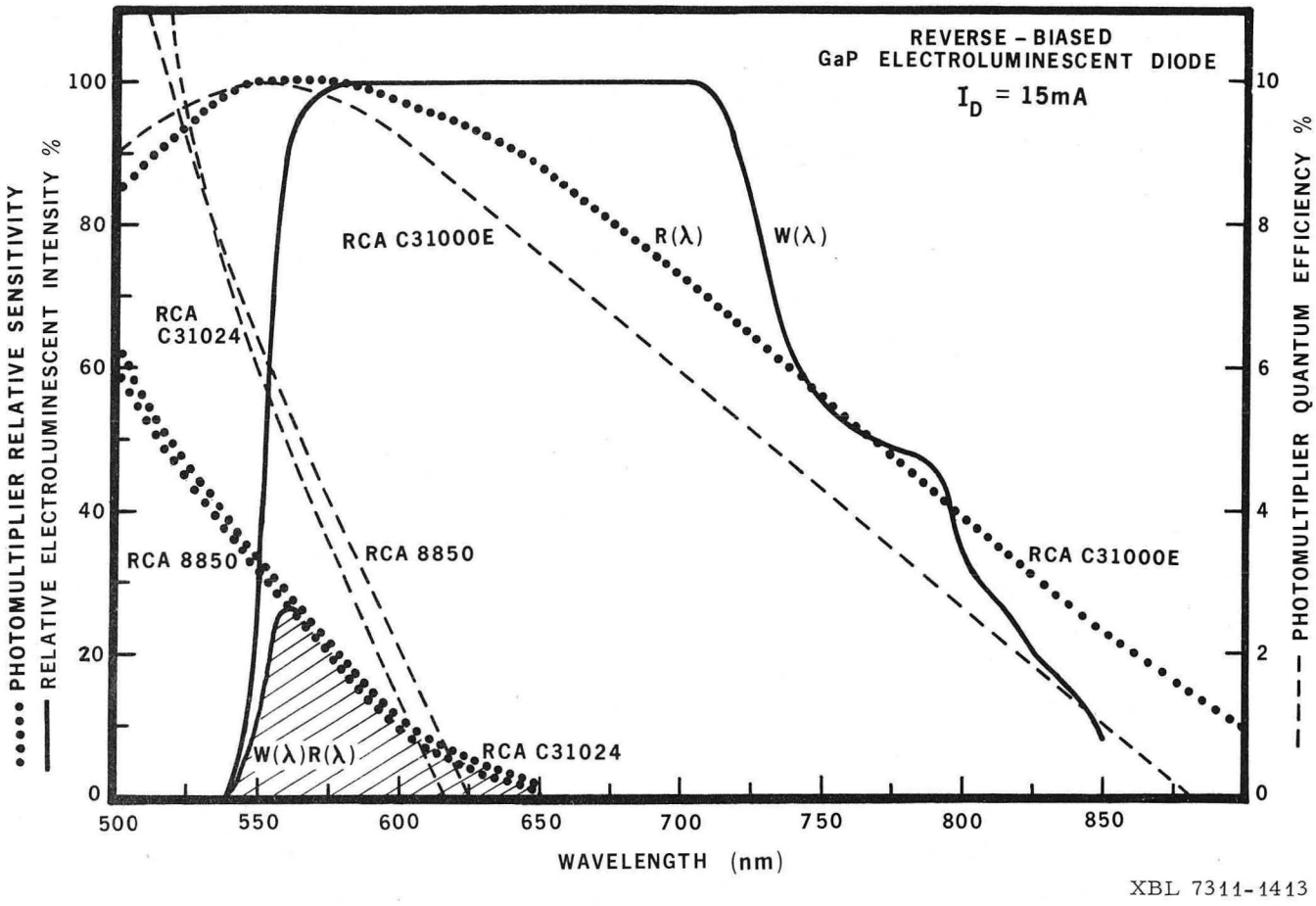

Fig. 3 Relative spectral characteristics of a reverse-biased gallium phosphide electroluminescent diode, Ferranti XP-23.

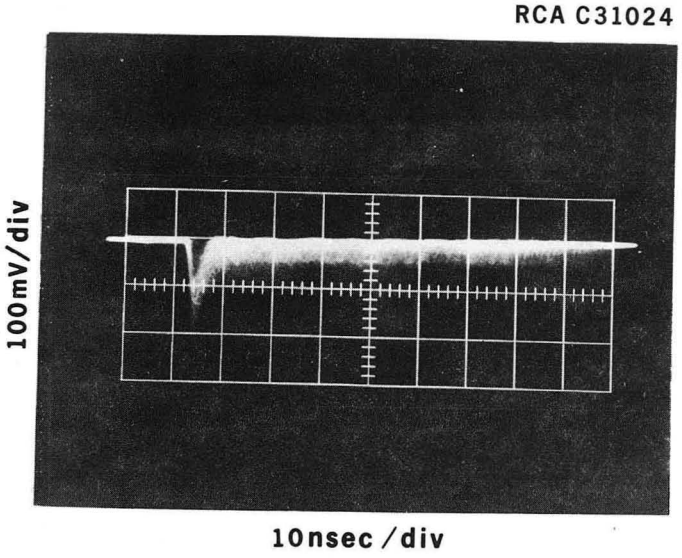

Fig. 4 Output pulses from a photomultiplier RCA C31024 operated at 3.5 kV using a 250 psec impulse excitation from an electroluminescent diode in the forward direction. The vertical scale is 100 mV per division and the time scale is 10 nsec per division.

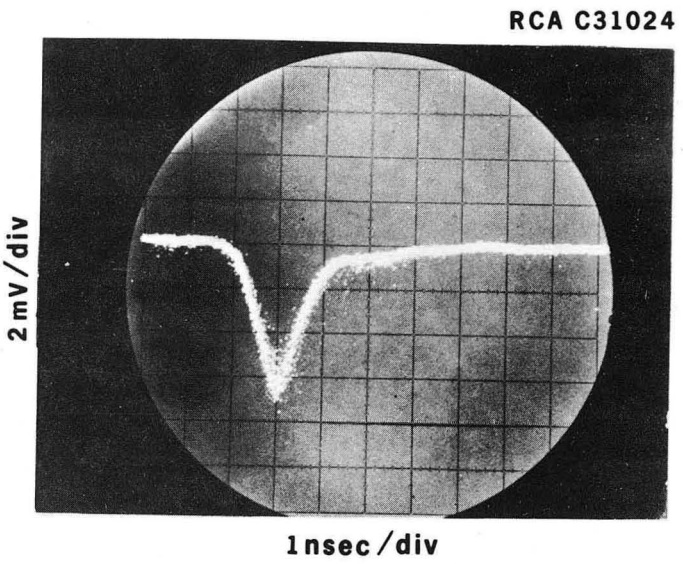

Fig. 5 Single photoelectron pulses from an RCA C31024 operated at 3.5 kV using a 200 psec impulse excitation from an electroluminescent diode in the reverse direction. The vertical scale is 2 mV per division and the time scale is 1 nsec per division.

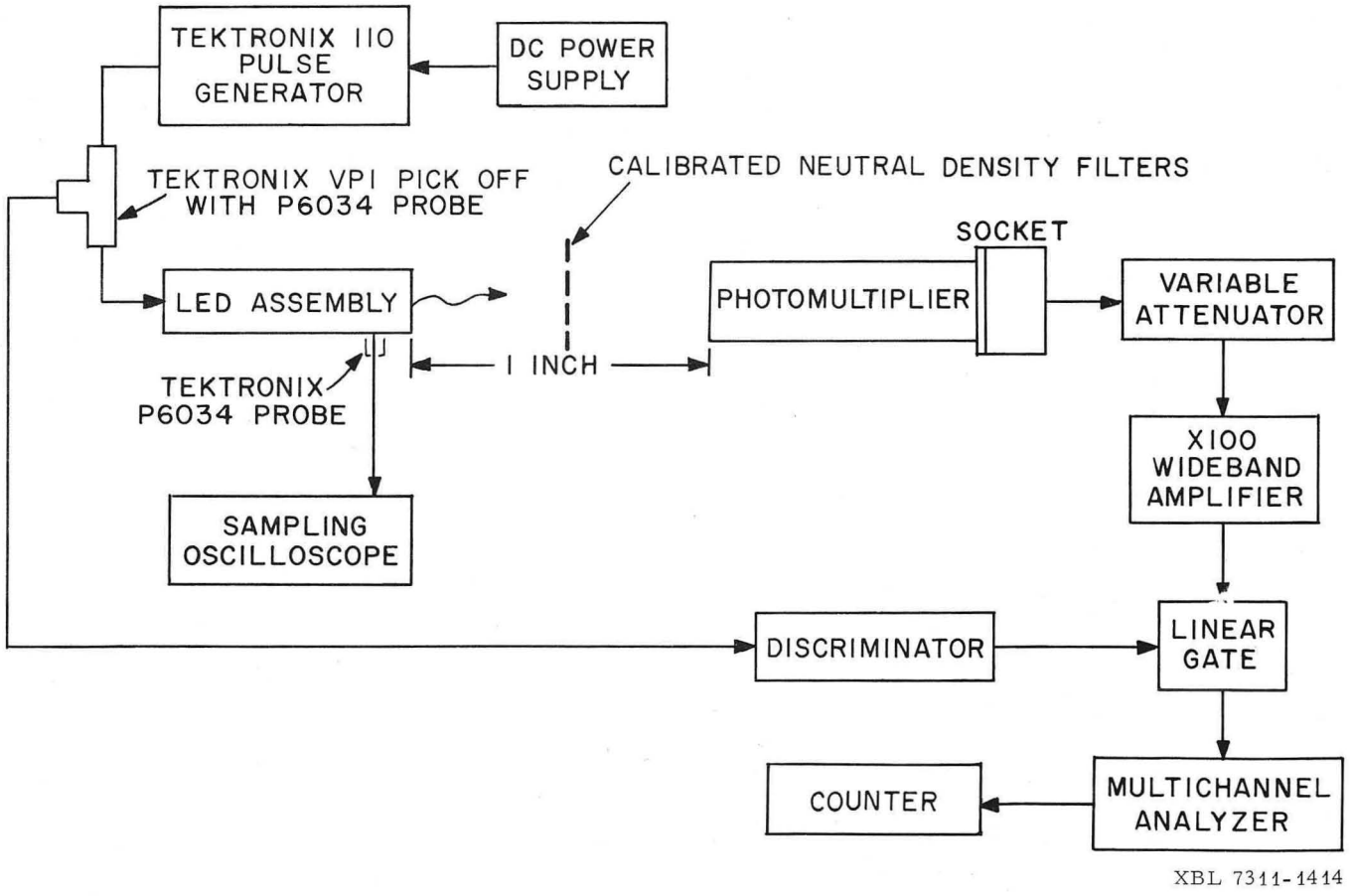

Fig. 6 Block diagram of the system for measuring photoelectron yield per pulse as a function of electroluminescent diode pulse current.

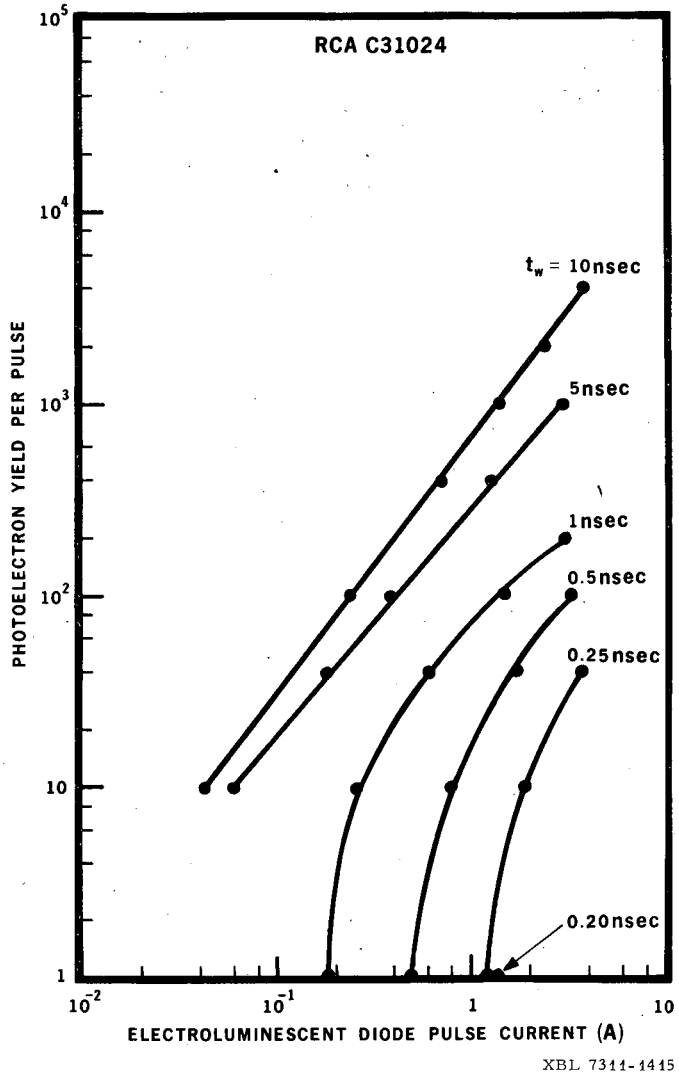

Fig. 7 The photoelectron yield per pulse from an RCA C31024 as a function of electroluminescent diode pulse current, with current pulse width as the parameter.

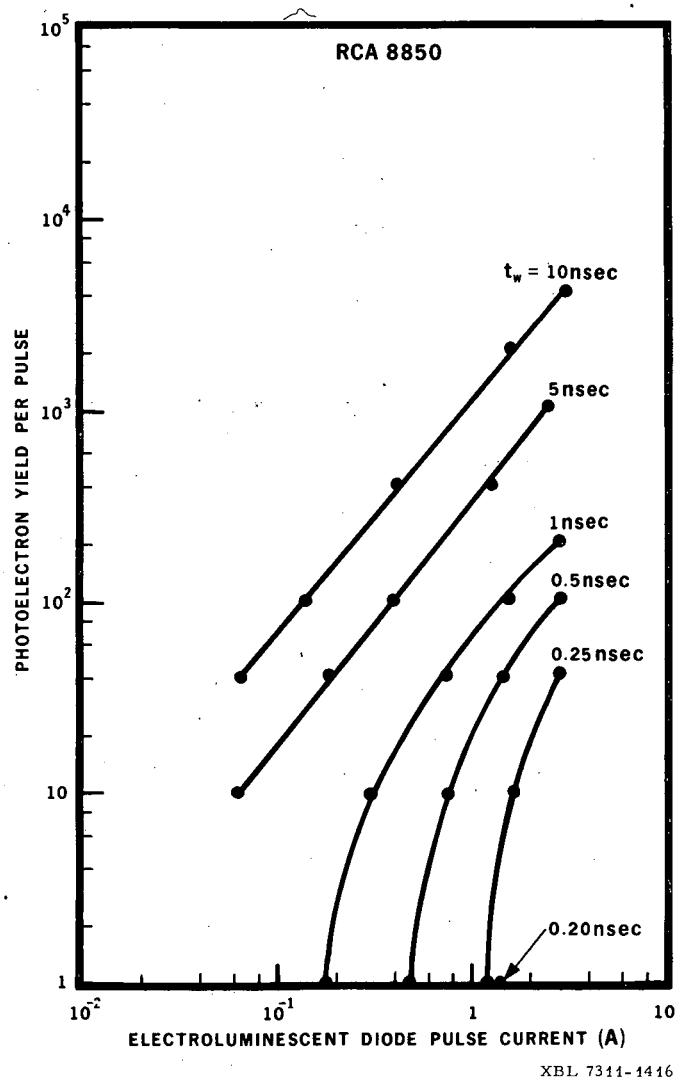

Fig. 8 The photoelectron yield per pulse from an RCA 8850 as a function of electroluminescent diode pulse current, with current pulse width as the parameter.

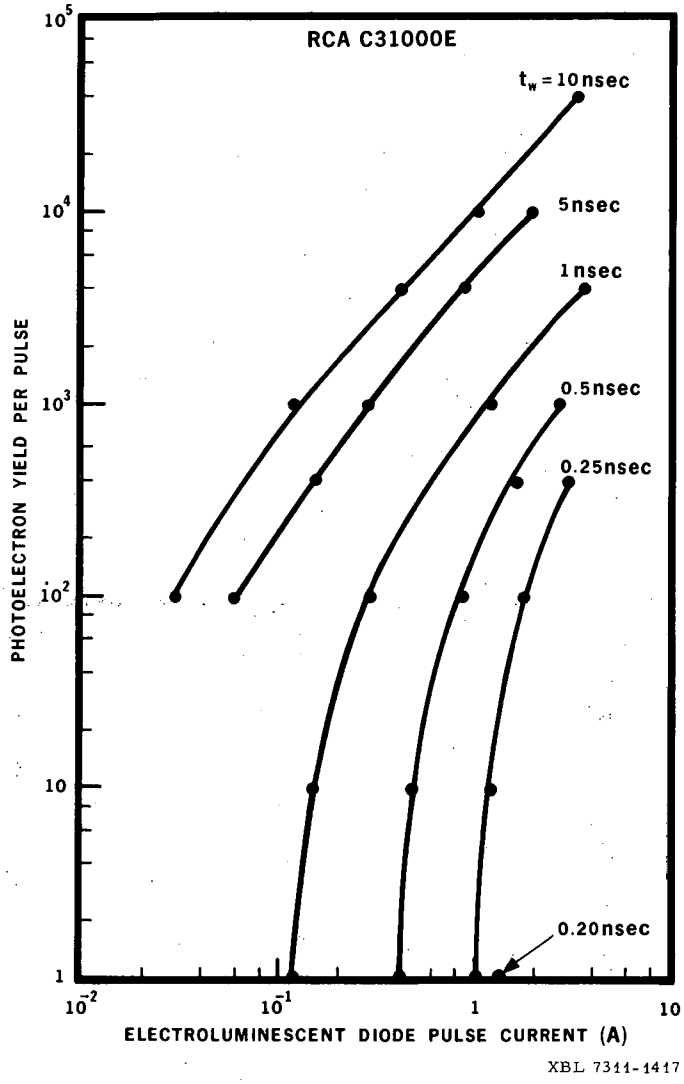

Fig. 9 The photoelectron yield per pulse from an RCA C31000E as a function of electroluminescent diode pulse current, with current pulse width as the parameter.

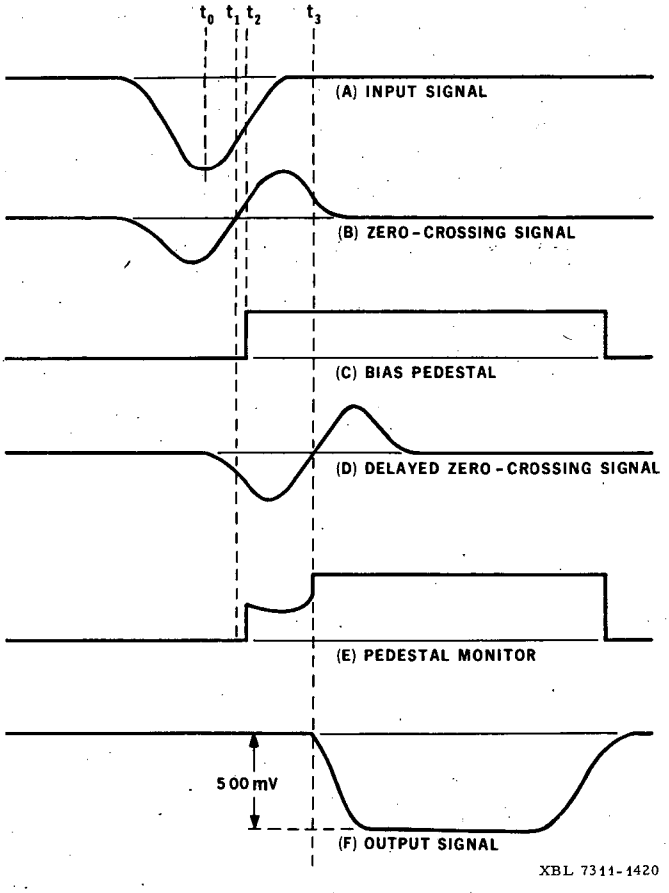

Fig. 12 Waveforms at the specified points in the schematic diagram of Fig. 11.

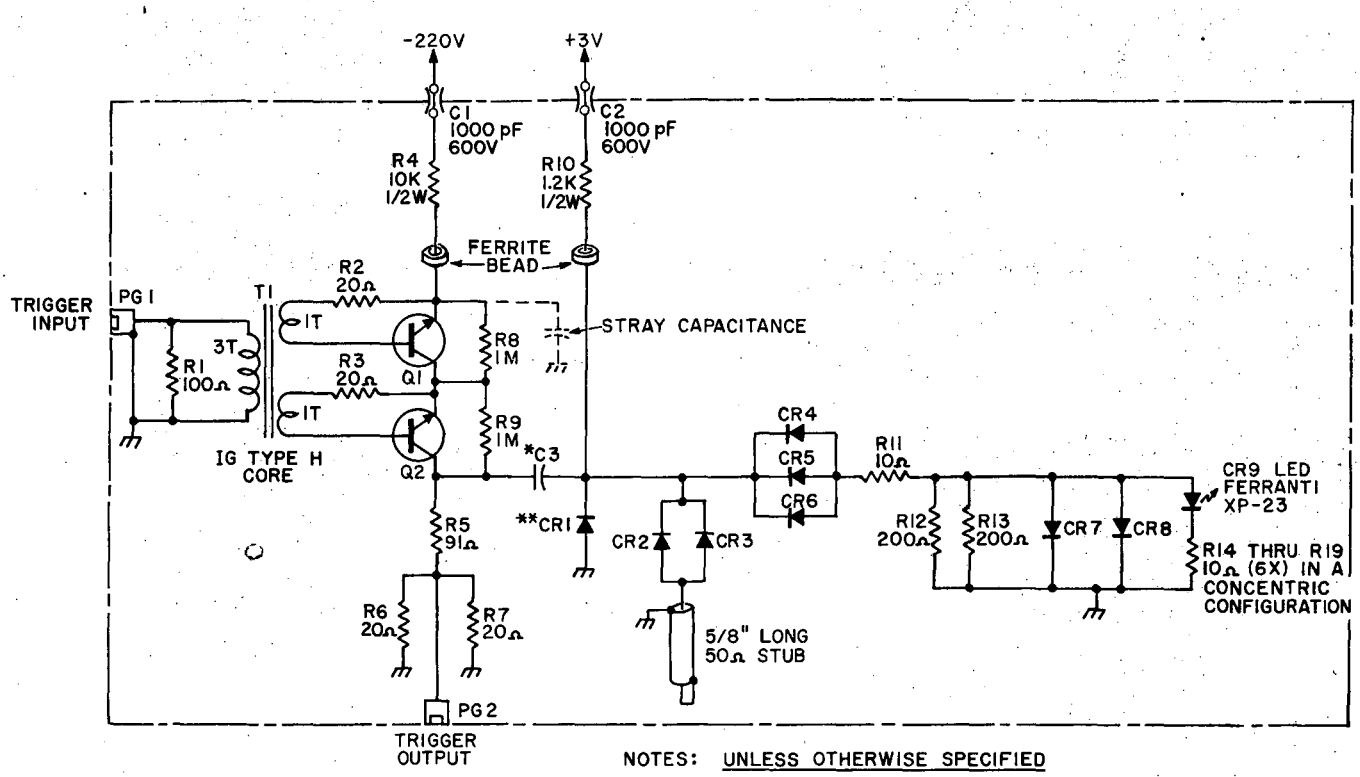

NOTES: UNLESS OTHERWISE SPECIFIED

1. DIODES HPA 5082-2303
2. RESISTORS 1/4 W 5% CARBON COMPOSITION
3. TRANSISTORS 2N2222
**4. CR1 HPA 5082-0320
*5. MICRO-STRIP CAPACITOR 470 pF 200V AMERICAN TECHNICAL CERAMIC ATC-100 B 471 M MS 200

XBL 7311-1418

Fig. 10 Schematic diagram of the subnanosecond light pulse generator.

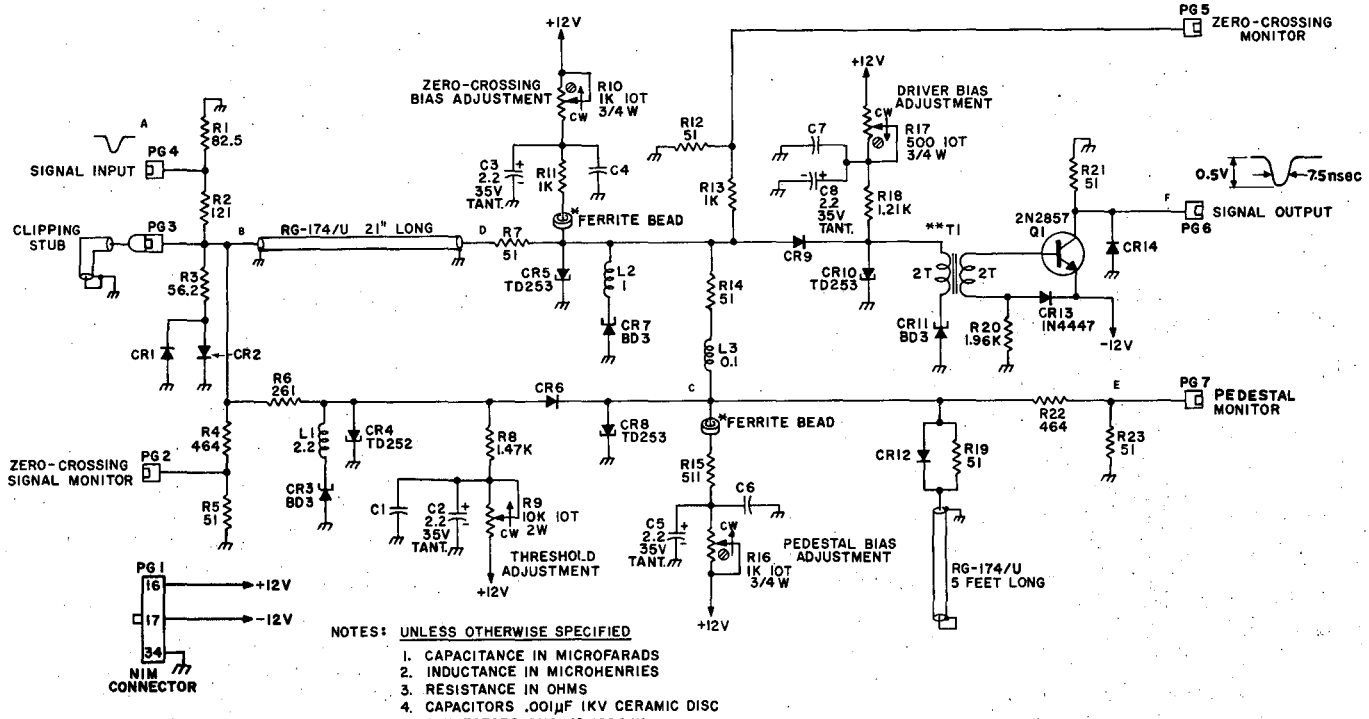

NOTES: UNLESS OTHERWISE SPECIFIED

1. CAPACITANCE IN MICROFARADS
2. INDUCTANCE IN MICROHENRIES
3. RESISTANCE IN OHMS
4. CAPACITORS .001μF 1KV CERAMIC DISC
5. CONNECTORS BNC UG-1094/U
6. DIODES HPA 5082-2303
7. RESISTORS 1/8W 1% METAL FILM
*8. FERRITE BEADS FERROXCUBE NO. 56-590-65
**9. T1 TOROIDAL CORE INDIANA GENERAL CF102 TYPE H

XBL 7311-1419

Fig. 11 Schematic diagram of the zero-crossing discriminator.

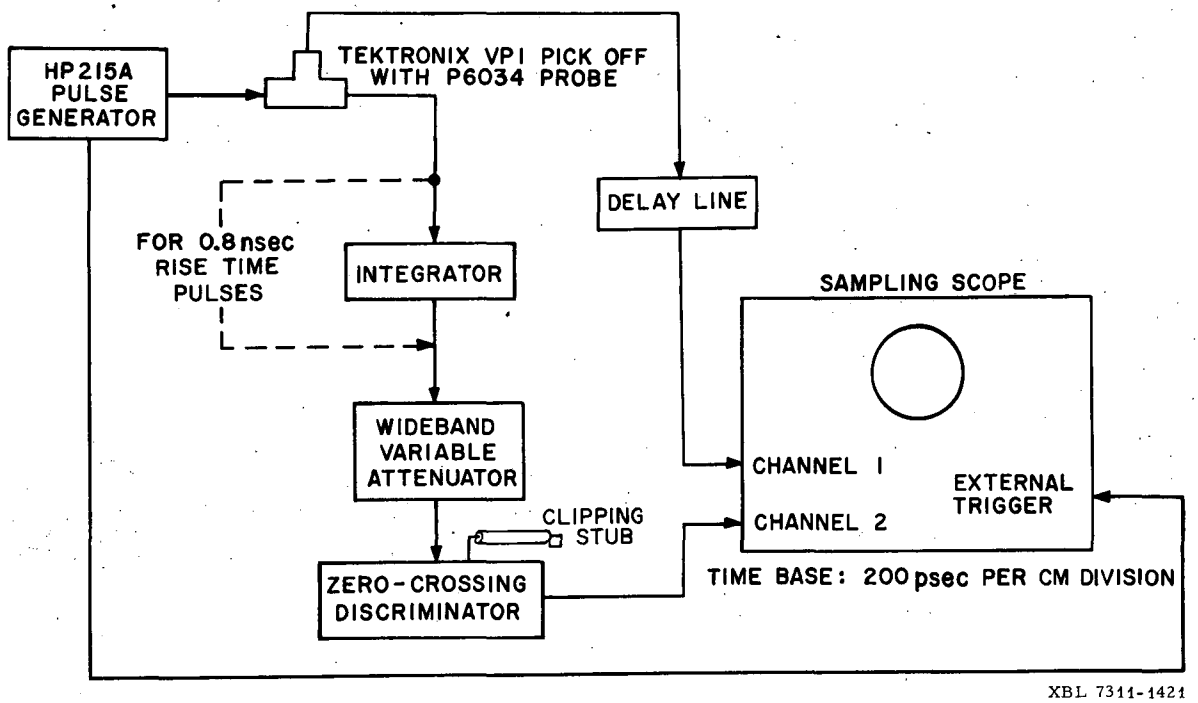

Fig. 13 Block diagram of the system for measuring discriminator time-walk characteristics.

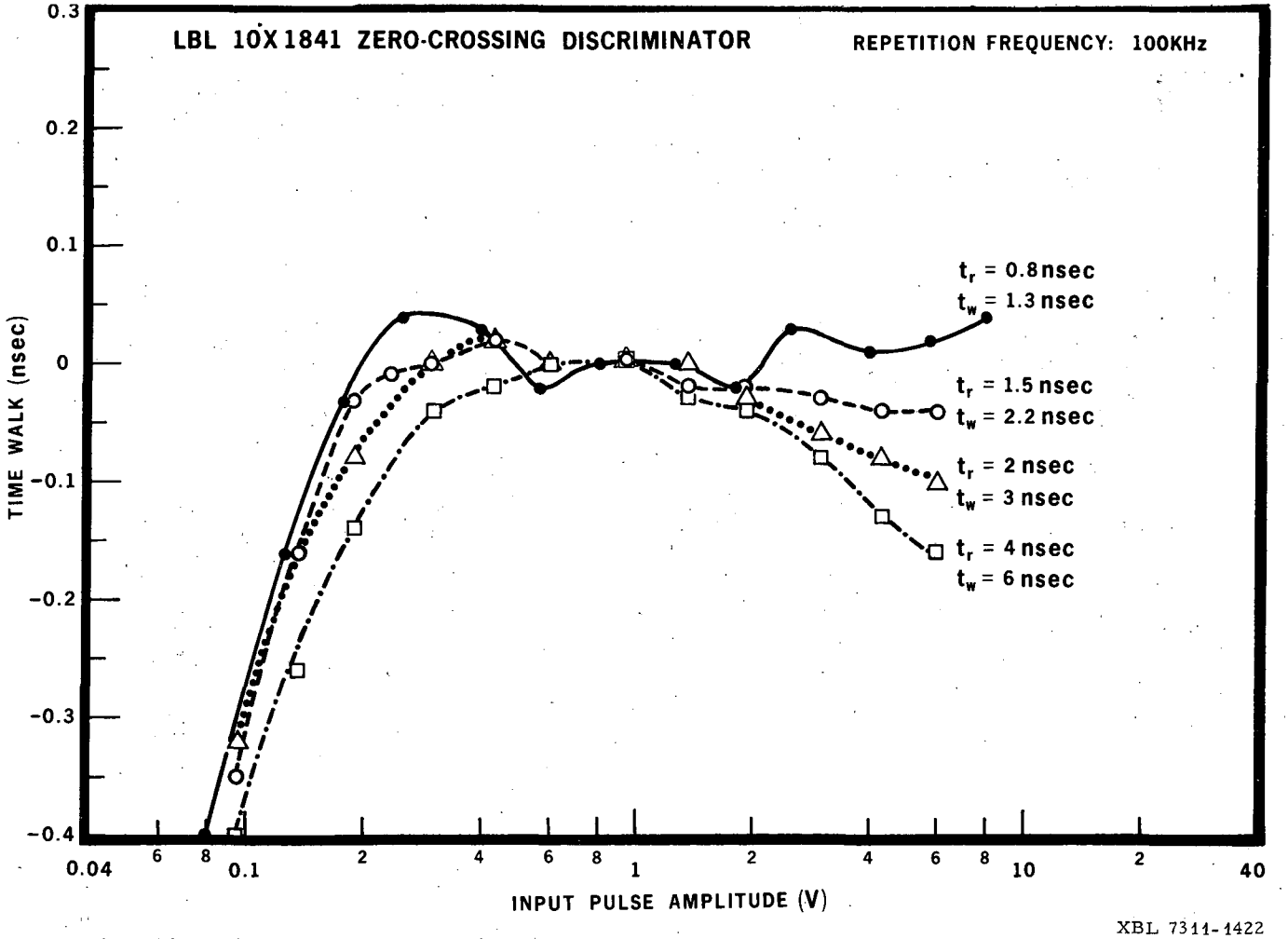

Fig. 14. Time-walk characteristics of the zero-crossing discriminator as a function of the input pulse amplitude, with impulse pulse rise time and width as parameters.

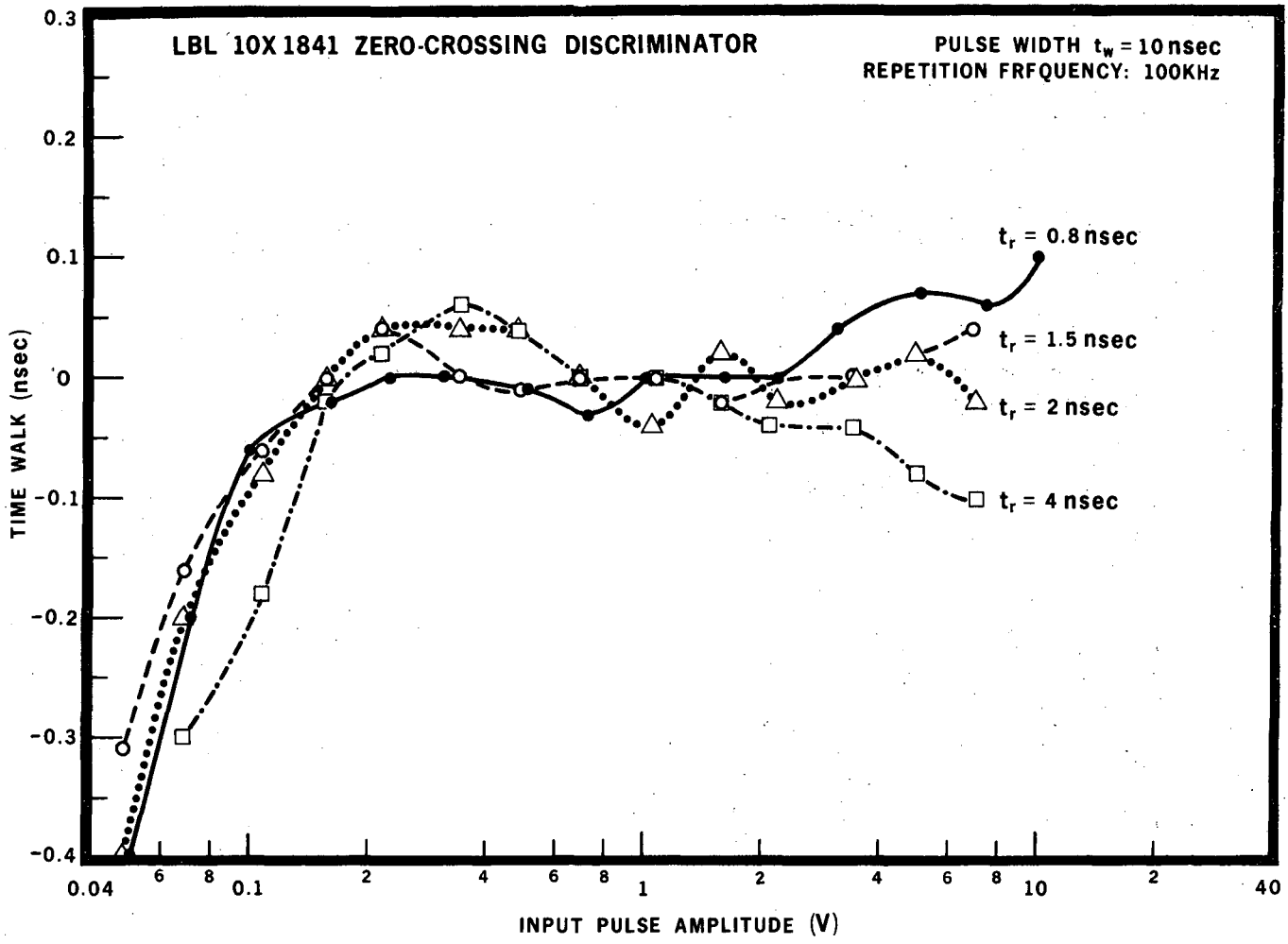

XBL 7311-1423

Fig. 15 Time-walk characteristics of the zero-crossing discriminator with an input pulse amplitude width t_w = 10 nsec, and pulse risetime as a parameter.

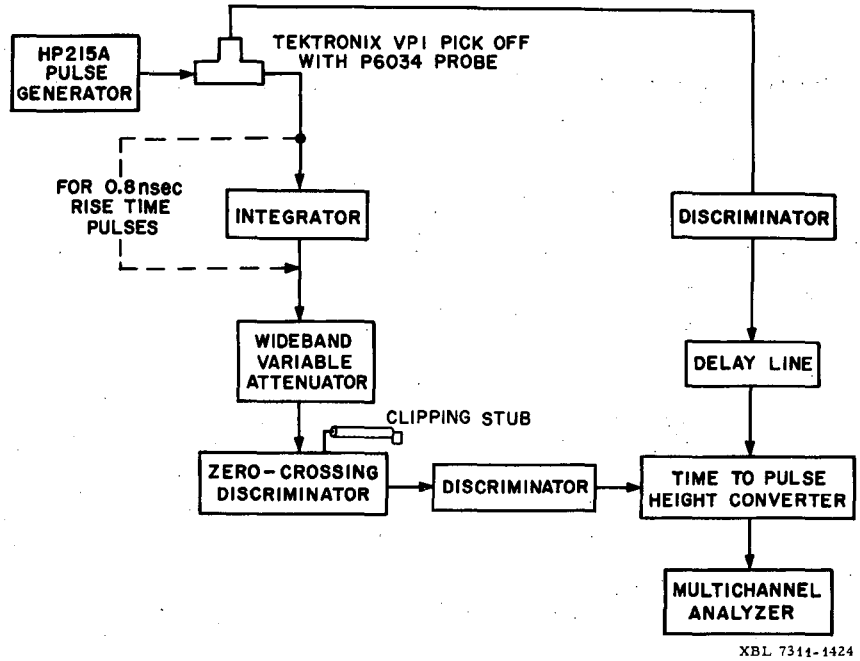

XBL 7311-1424

Fig. 16 Block diagram of the system for measuring the time resolution of the zero-crossing discriminator.

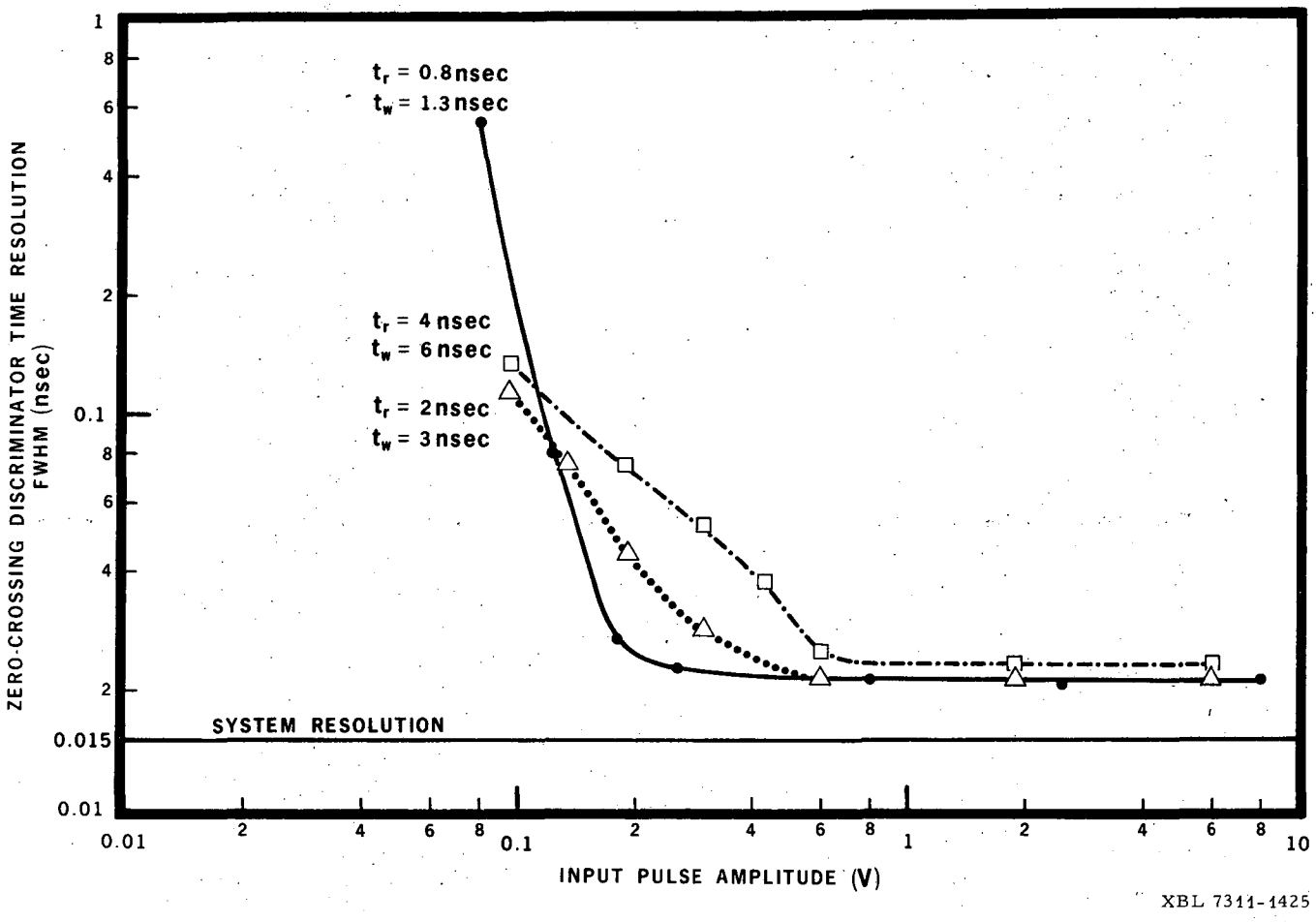

Fig. 17 Discrimination time resolution characteristics as a function of the input pulse amplitude, with input pulse rise time and width as parameters.

TECHNICAL INFORMATION DIVISION
LAWRENCE BERKELEY LABORATORY
UNIVERSITY OF CALIFORNIA
BERKELEY, CALIFORNIA 94720